since 1961

Baltica

BALTICA Volume 39 Number 1 June 2026: 41–57
https://doi.org/10.5200/baltica.2026.1.5

Research article

Study on the effect of freeze-thaw action on the mechanical strength and microstructure of improved peat soil in Zoige seasonal frozen area

Yiying Cui, Min Xia*, Shanyun Tang, Qi Huang

Cui, Y., Xia, M., Tang, Sh., Huang, Q. 2026. Study on the effect of freeze-thaw action on the mechanical strength and microstructure of improved peat soil in Zoige seasonal frozen area. *Baltica 39(1)*, 41–57. Vilnius. ISSN 1648-858X.
Manuscript submitted 18 June 2025 / Accepted 31 March 2026 / Available online 24 April 2026

Abstract. To investigate the frost damage of Zoige Plateau Peat Permafrost and the stability of engineering foundations in seasonally frozen regions, this study builds upon previous research on the optimal mix ratio of composite stabilized peat soil using mineral powder-steel slag and basalt fibre as primary materials, supplemented with polycarboxylate superplasticizer and carbide slag. Indoor mechanical tests (unconsolidated undrained triaxial shear test, unconfined compressive strength test, and scanning electron microscopy test) were conducted on stabilized soils subjected to varying freezing temperatures and freeze-thaw cycles to explore the mechanical properties and microscopic mechanisms under freeze-thaw action. Based on the experimental dataset, the peak strength of stabilized peat soil was predicted using a particle swarm optimization backpropagation neural network (PSO-BP). The results indicate that the unconfined compressive strength and residual strength ratio of stabilized peat soil are positively correlated with freezing temperature and negatively correlated with the number of freeze-thaw cycles. The stress-strain curve characteristics of stabilized peat soil are generally consistent under different conditions. With increasing cycles, the peak strength and cohesion of the stabilized peat soil first decrease and then stabilize, while the internal friction angle remains relatively unchanged. In the peak strength model constructed using MATLAB, the PSO-BP neural network model exhibited a higher correlation coefficient (R^2) and better overfitting performance compared to the BP neural network model, enabling a more accurate strength prediction of stabilized peat soil.

Keywords: *freeze-thaw cycle; unconfined compressive strength; unconsolidated undrained test; scanning electron microscopy; model prediction*

Yiying Cui (2317679038@qq.com),
Min Xia (xiamin15@cdut.edu.cn, https://orcid.org 0000-0003-3621-3422),*
Shanyun Tang, Qi Huang
State Key Laboratory of Geological Disaster Prevention and Geoenvironment Protection (Chengdu University of Technology), Chengdu 610059, China
**Corresponding author*

INTRODUCTION

The Zoige Plateau is located in the north-eastern part of the Qinghai-Tibet Plateau and contains the largest peat deposit in China. The region experiences long winters with no summer, with minimum temperatures reaching as low as -20°C. Additionally, the Zoige Plateau is characterized by a relatively low latitude, high elevation, and intense sunlight. However, peat soils in seasonally frozen regions are subject to severe freeze-thaw damage under the influence of varying freezing temperatures, which can lead to irreversible effects on soil strength and deformation characteristic (Fan *et al*. 2023). At the same time, it poses significant challenges to the stability of engineering foundations and constitutes a critical issue for large-scale infrastructure development in western China. Therefore, investigating the improvement and reuse of peat soils in seasonally frozen regions is essential for mitigating permafrost-related damage.

In recent years, limited research has been conducted on the mechanical properties of modified

peat soils in seasonally frozen regions. Studies often adopt analogical methods based on the mechanical properties of other freeze-thaw soils to explore the effects of freeze-thaw cycles on soil characteristics. Ding *et al*. (2024a) studied the effects of freeze-thaw (F-T) cycles on the mechanical properties and bearing capacity of strongly chlorine saline soil from the Qarhan Salt Lake region. F-T cycles cause volume reduction in low-density soil and expansion in high-density soil due to particle breakage and reaggregation. Compacted soil deteriorates significantly after high-frequency F-T cycles, affecting foundation performance. Ding *et al*. (2024b), Fan *et al*. (2024a), also Zhang and Han (2024) conducted unconsolidated undrained (UU) tests on reconstituted soils under different confining pressures and freeze-thaw cycles. Their results showed that the peak strength of the samples increased with confining pressure, while the cohesion and peak strength decreased with more freeze-thaw cycles, with only minimal change in the internal friction angle. In summary, existing research indicates that freeze-thaw cycles exert detrimental effects on both the compressive and shear strength of soils. Consequently, there is a pressing need to develop innovative soil improvement techniques to enhance stability in seasonally frozen regions.

Hou *et al*. (2025) studied the freeze-thaw resistance of HPMC-modified loess through triaxial testing. The study found that stress-strain behaviour varies with confining pressure, showing hardening at lower pressures and softening at higher pressures. Peak stress and shear strength initially decrease, then increase, and stabilize. Yang *et al*. (2022) researched that sludge-solidified lightweight soil undergoes rapid strength loss during the first two freeze-thaw cycles, accounting for 78% of total attenuation. After eight cycles, strength stabilizes as the soil structure becomes more stable, transitioning from strong to weak strain-softening. Feng *et al*. (2010) investigated the relationship between mixed fillers and freeze-thaw damage with factors such as freeze-thaw cycles, freezing temperature, and porosity. Their study revealed that increased freeze-thaw cycles and lower freezing temperatures significantly reduce the stability and splitting strength of solidified soil. Kalkan *et al*. (2022) investigated the effects of quartzite on the freeze-thaw resistance of clayey soil from Erzurum, NE Turkey. The study revealed that adding quartzite improved mechanical properties and freeze-thaw resistance by reducing permeability and increasing shear strength. These findings suggest that quartzite is an effective natural additive for stabilizing clayey soils in cold regions, enhancing their suitability for geotechnical applications. Shao *et al*. (2022) studied the strength changes of soft soil stabilized by GGBS (Ground Granulated Blast Furnace Slag) and alkaline activators (lime) under freeze-thaw cycles. The unconfined compressive strength tests indicated that the strength of the stabilized soil under freeze-thaw cycles was lower than that under standard curing conditions. Kan *et al*. (2024) investigated the frost resistance of soil stabilized with slag/fly ash in an alkaline environment under freeze-thaw cycles. The results showed that the frost resistance and compressive strength of the modified soil improved after stabilization.

Chai and Zhang (2023) conducted SEM tests on soil modified with alkali-activated fly ash and mineral powder after undergoing dry-wet and freeze-thaw cycles. The results indicated that the modified expansive soil had limited pore expansion and crack development, maintaining soil integrity and enhancing strength compared to the original soil. Research by Chen *et al*. (2019) revealed that the fractal dimension of soil pore structure decreases with more freeze-thaw cycles, simplifying the structure. After 20 cycles, higher freezing temperatures increase pore complexity. In the early stages, at -5°C, the pore structure is more complex than at lower temperatures (-10°C, -15°C). Although considerable efforts have been devoted to analysing the effects of freeze-thaw cycles on stabilized soils, including microstructural changes and strength variation mechanisms, there is still a lack of research on the strength evolution and shear strength prediction of improved peat soils under freeze-thaw conditions.

The applicability of novel composite materials is often influenced by multiple interacting factors, including material content and environmental conditions. In ecologically fragile regions, the heterogeneity and anisotropy of soil exhibit complex, multidimensional nonlinear relationships, making it difficult for traditional orthogonal experiments to ensure accuracy. Therefore, a more precise model is required to predict soil strength. Li *et al*. (2023) explored the effects of freeze-thaw cycles on the compressive strength of stabilized saline soil. A nonlinear fitting model and a neural network-based strength damage model were developed with compaction, moisture content, and freeze-thaw cycle number as influencing factors. The results showed that the neural network model had higher fitting accuracy and applicability. The stabilization mechanisms of silty clay improved with optimal proportions of GGBS, FA, and lime under freeze-thaw cycles were systematically investigated. Based on these findings, a high-precision predictive model for unconfined compressive strength (UCS) was established. The PSO-BP model demonstrated superior performance, achieving a coefficient of determination (R^2) of 0.982 on the test set, thereby providing a reliable reference for evaluating soil stability in seasonally frozen regions (Sun *et al*. 2025). A one-part geopolymer (OPG) was employed as an alternative soil stabilizer to replace conventional ce-

ment, and its durability under freeze-thaw conditions was systematically evaluated. A small dataset comprising 216 data points was utilized, and three deep learning models were developed to simulate and predict the strength performance of OPG-stabilized soils subjected to freeze-thaw cycles. Among the models, the convolutional neural network (CNN) exhibited the best predictive performance, achieving a coefficient of determination (R^2) of 0.9966. Furthermore, the model provides the capability to interpret the influence of input variables on the prediction outcomes (Yao *et al.* 2024).

In conclusion, many scholars have studied the mechanical properties and microstructure of stabilized soil under freeze-thaw cycles and established damage models to simulate the effects of freeze-thaw cycles on soil strength. However, research on stabilized peat soils in seasonally frozen regions is still limited. Specifically, the macroscopic and microscopic deterioration mechanisms under freeze-thaw cycles have not been comprehensively elucidated, and predictive models for shear strength under different freeze-thaw conditions are lacking. Therefore, this study focuses on peat soil in the Zoige Plateau of the seasonally frozen region, simulating local climatic conditions to conduct freeze-thaw cycle tests. The study analyzes the mechanical strength and microstructure of stabilized peat soil. Unconfined compressive strength tests and unconsolidated undrained triaxial shear tests are conducted to analyze the variations in mechanical strength and associated parameters. Additionally, scanning electron microscopy (SEM) tests are performed to observe the micro-damage mechanisms within the soil samples. Meanwhile, we study the shear strength behaviour of solidified peat soil under freeze-thaw cycles, compare the prediction models of multiple linear regression (MLR), backpropagation (BP) neural network and particle swarm optimization-enhanced BP (PSO-BP) neural network, and systematically evaluate their prediction accuracy and generalization ability.

MATERIALS AND METHODS

Specimen preparation

The soil samples were collected from the peat swamp near National Highway 213 in Zoige County (Fig. 1). To obtain undisturbed samples, soil was sampled from a depth of 0 to 2 meters below the sur-

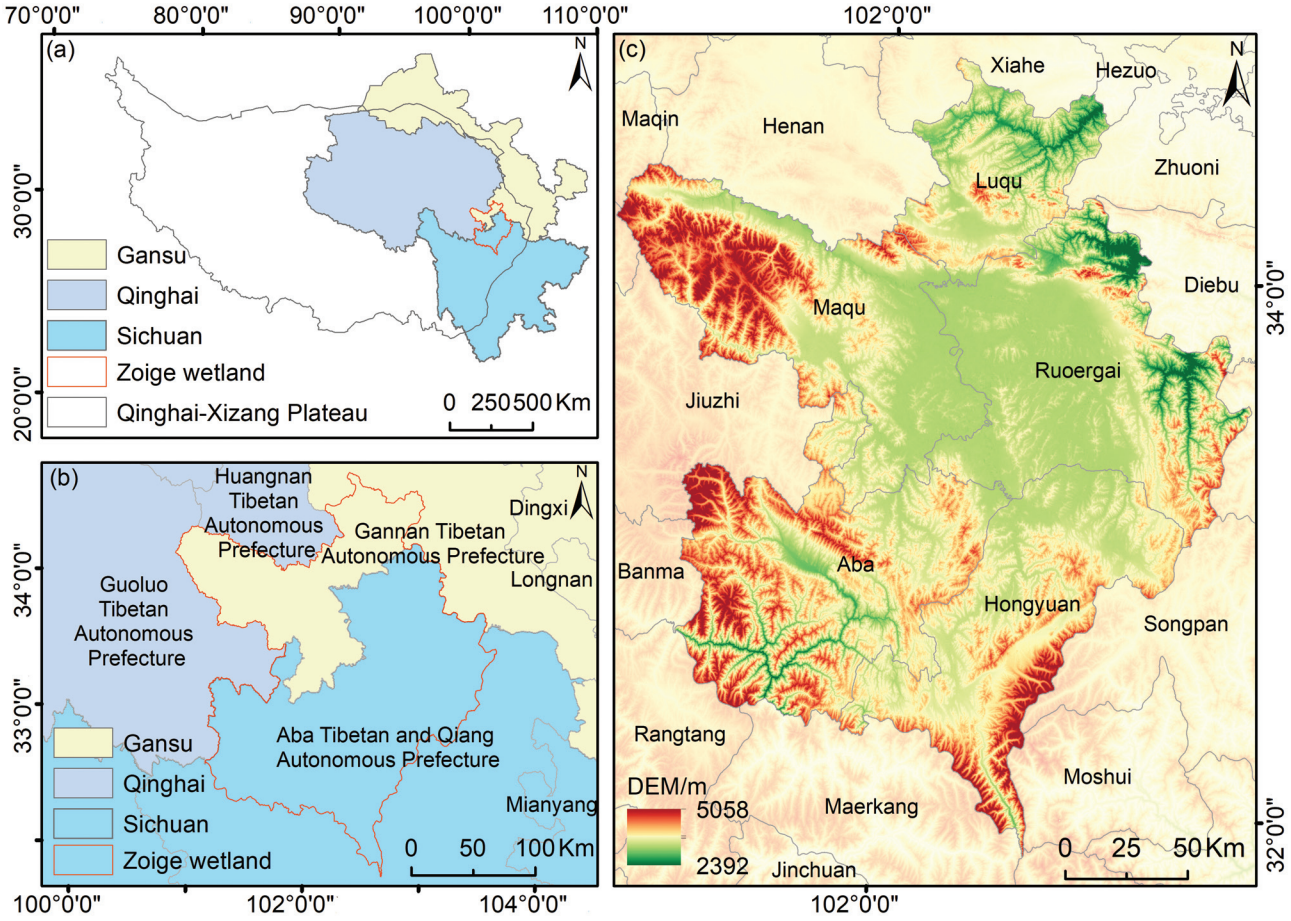

Fig. 1 Location map of the Zoige Plateau study area in the eastern Tibetan Plateau, China. The map shows the geographic coordinates and the position of the sampling sites

Table 1 Physical and mechanical properties of specimens

Natural water content /%	Optimum moisture content /%	Maximum dry density /(g·cm^{-3})	Liquid limit /%	Plastic limit /%	Void ratio	Specific gravity	Organic content /(%)	PH
65.39	38.5~40.6	0.96	73.58	40.37	0.69	1.61	22.31	6.5

Table 2 Main chemical composition table of curing materials

	Al_2O_3	SiO_2	CaO	MgO	Fe_2O_3
Fly ash	30%	50%	10%	4.3%	3.2%
Carbide slag	2.2%	3.4%	85%	1.5	1.2%
Slag powder	16.70%	34.5%	35.3%	5.01%	1.5%
Steel slag powder	10.97%	23.65%	38.19%	7.96%	12.17%

face by using a thin-walled cylindrical sampler with a diameter of 10 cm and height of 20 cm. The sampler was driven into the soil layer along a vertical direction under static pressure for continuous sampling. The materials used in the peat soil improvement study conducted by the research team include Zoige Plateau peat soil, steel slag, mineral powder, carbide slag, water reducer, basalt fibre, and tap water.

Zoige Plateau peat soil is a special type of soil, primarily composed of organic matter and moisture, with the organic content of peat reaching up to 90%. It is characterized by a high porosity, high moisture content, low bearing capacity, high compressibility, low permeability, and poor engineering mechanical properties. The basic physical properties of the peat soil were determined using standard geotechnical testing methods, and the results in Table 1 represent the averaged values for the study area.

Based on earlier research conducted by the team on soil improvement, the optimal mix proportions were obtained from preliminary tests conducted by our group (Tang *et al.* 2027). The optimal mix ratio for stabilized peat soil was determined to be: steel slag: GGBS: basalt fibre: water reducer: carbide slag = 10.67%: 9.33%: 0.25%: 0.2%: 15%. Thus, this optimal mix ratio was used for the stabilized soil samples in the current study. The main chemical components of the curing materials used in the experiments are shown in Table 2.

Test methods

The collected peat soil was first ground and placed in an oven at 50°C for low-temperature drying. After drying, the soil was sieved through a 2 mm mesh and stored in a sealed dry container for later use.

1. Preparation of original peat soil: A light compaction test was performed. Based on the liquid and plastic limits of the peat soil, the optimal moisture content of 40% and a maximum dry density of 1.0 g·cm³ were used as preparation standards. Water, equal to 40% of the dry weight of the soil, was added to the dried peat soil and thoroughly mixed. Moisture content was then measured.

2. Preparation of stabilized peat soil: The dried peat soil, steel slag powder, mineral powder, basalt fibre, polycarboxylate superplasticizer, and carbide slag were mixed according to the optimal ratio in a blender for 2 minutes. The predetermined amount of water was then added evenly and mixed thoroughly.

3. The two types of soil samples were placed in a mold with a diameter of 39.1 mm and a height of 80 mm in five layers. Each layer was compacted for 2 minutes using a vibrating table until no air bubbles were visible. Once the specimens were formed, they were sealed with plastic wrap. After 24 hours, the mold was removed, and the samples were placed in a standard curing box set at a temperature of 20 ± 5°C and humidity ≥ 95% for 28 days of curing.

Experimental scheme

To investigate the effect of natural environmental conditions in seasonally frozen regions on the mechanical strength of stabilized peat soil, a two-factor comprehensive experiment was conducted, with freezing temperature and freeze-thaw cycles as experimental variables. The freeze-thaw cycles were tested using a fully automated freeze-thaw testing machine. Based on the temperature variations of the Zoige Plateau seasonally frozen region, the freezing temperatures were set at -20°C, -10°C, and -5°C, with a melting temperature set at 20°C (room temperature). One freezing and one melting process were considered as one complete freeze-thaw cycle. Both freezing and melting times were set to 12 hours. The number of freeze-thaw cycles was set to 0, 1, 3, 5, 10, 15, 30, and 60 cycles. After each freeze-thaw cycle, the soil samples were subjected to the following tests Fig. 2):

1. Unconfined compressive strength test: A shear rate of 1 mm/min was applied to determine the compressive strength and residual strength ratio of the samples. For each mix proportion, three replicate specimens were tested, and the reported values are the averages of the three tests.

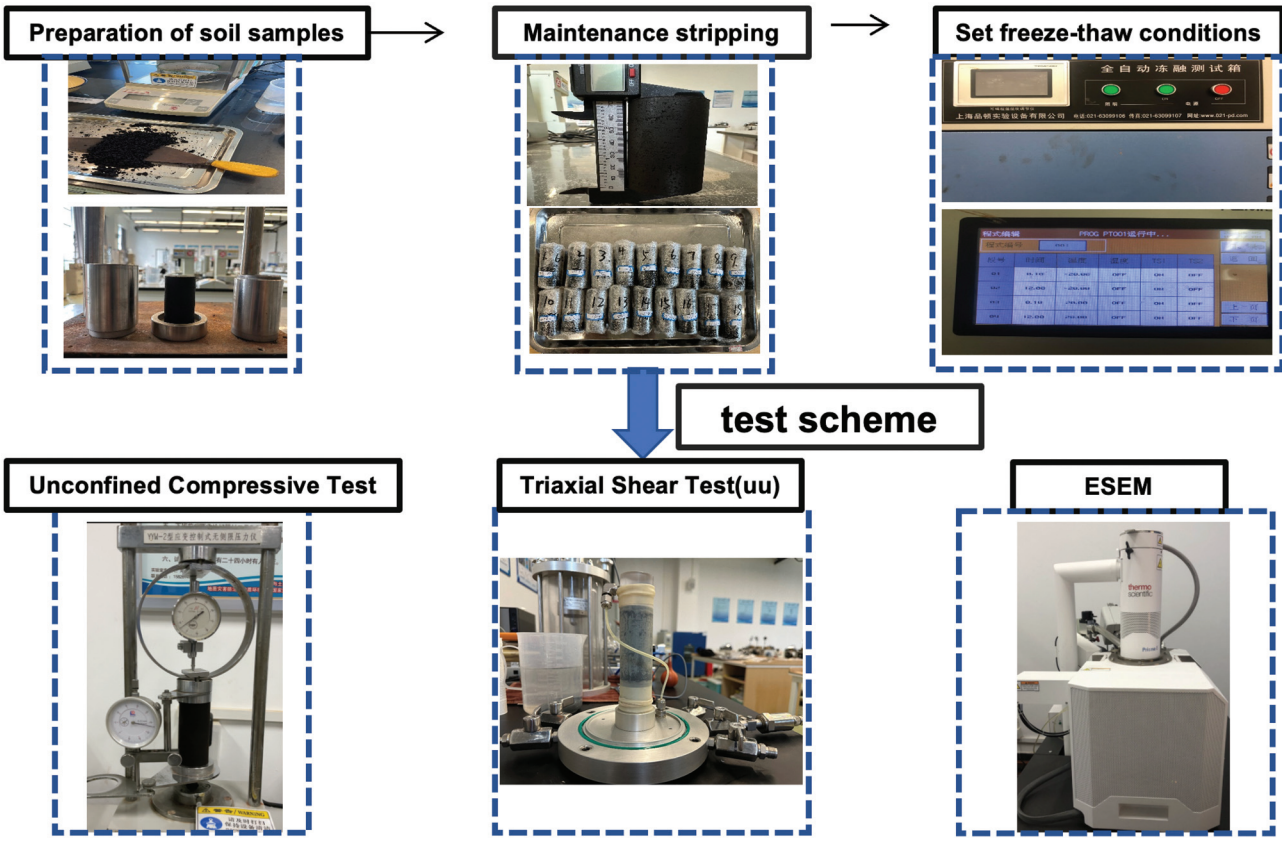

Fig. 2 *Sc*hematic diagram of sample preparation, freeze-thaw cycles, unconfined compressive strength (UCS) test, UU triaxial test, and scanning electron microscopy (SEM) analysis

2. Unconsolidated undrained (UU) test: Since freeze-thaw cycles primarily affect the surface layer of the foundation, and the low permeability of peat soil usually prevents drainage consolidation during the melting phase, a UU test was conducted under pre-set confining pressures of 100 kPa, 200 kPa, and 300 kPa. The strain rate was set to 0.8 mm/min. For each confining pressure and mix proportion, three replicate specimens were tested, and the reported values are the averages of the three tests.

3. Scanning electron microscopy (SEM) test: The soil samples were subjected to SEM analysis after freeze-thaw cycles. Samples were dried, polished, and cut into 2 mm × 2 mm × 1 mm pieces for the test. For each freeze-thaw condition, one representative specimen was selected, and multiple images were captured at magnifications of 500× to 1000× to examine the internal microstructure. The selected specimen was representative of the corresponding mix proportion and freeze-thaw treatment.

EXPERIMENTAL RESULTS ANALYSIS

Unconfined compressive strength

For each freeze-thaw condition, three parallel specimens were tested, and the data presented in Fig. 3 are the average values of the three replicate tests. The error bars represent the dispersion of the test results. As shown in the figure, a relatively small error range indicates good repeatability of the experiments, and thus the variation trend of the residual strength ratio can be considered reliable. Figure 3 shows the unconfined compressive strength (UCS) of peat-stabilized soil under different freeze-thaw cycle counts (1, 3, 5, 10, 15, 30, 60) and various freeze-thaw temperatures (-20°C, -10°C, -5°C). Under the same freeze-thaw cycle count but different freezing temperatures, the UCS of the peat-stabilized soil decreased rapidly in the early stage and then gradually approached a stable level as the number of freeze-thaw cycles increased. For instance, at a freezing temperature of -20°C, after 1, 3, 5, 10, 15, 30, and 60 freeze-thaw cycles, the UCS decreased by 26.6%, 11.7%, 8.6%, 7.8%, 3.6%, 1.4%, and 1.3%, respectively. The results indicate that after a single freeze-thaw cycle, the soil experienced significant strength loss, with the greatest disturbance to the internal structure. However, as the number of freeze-thaw cycles increased, hydration reactions occurred within the soil, and the cementitious substances formed by volcanic ash reactions adhered to the pore surfaces, slowing down the deterioration caused by freeze-thaw damage. After one freeze-thaw cycle at -5°C, the strength of the stabilized peat

soil decreased from 1051.62 kPa to 847.33 kPa, a reduction of 19.9%. Similarly, after one freeze-thaw cycle at -10°C and -20°C, the UCS decreased to 823.46 kPa and 771.57 kPa, with reductions of 21.7% and 26.6%, respectively. These results show that the UCS of stabilized soil decreases as the freezing temperature decreases under freeze-thaw cycles. Shi *et al*. (2024) demonstrated that the unconfined compressive strength (UCS) of cement-fly ash-stabilized organic soils decreases continuously after freeze-thaw cycles, accompanied by a significant loosening of the pore structure. They attributed this deterioration mechanism to pore expansion and the weakening of cementitious structures induced by the frost heave-thaw settlement process. A 2024 study by Zhao *et al*. (2024) on cement-fly ash-stabilized organic soils also confirmed that freeze-thaw action leads to a reduction in the soil strength parameters, with the deterioration and damage being particularly pronounced during the initial cycles. The conclusions of the above studies are fundamentally consistent with the experimental laws obtained in this paper.

Figure 4 illustrates the variation in the residual strength ratio under different freeze-thaw temperatures and cycle counts. Residual strength refers to the final strength that stabilizes after the peak in the stress-strain curve of soil or rock, and the ratio of residual strength to the compressive strength at room temperature is defined as the residual strength ratio (Wan *et al*. 2018). For example, at a freezing temperature of -20°C, after 1, 3, 5, 10, 15, 30, and 60 freeze-thaw cycles, the residual strength ratio was 63.33%, 59.24%, 56.56%, 54.48%, 53.86%, 52.97%, and 51.23%, respectively. During freeze-thaw cycles, the water in the soil particle pores freezes and expands, leading to structural swelling and the formation of micro-cracks. Repeated freeze-thaw cycles further propagate these micro-cracks, loosening the soil structure, which is manifested macroscopically as reduced strength and a lower residual strength ratio. Previous studies on improved soils subjected to freeze-thaw conditions have also reported the same phenomenon: repeated freeze-thaw cycles reduce the peak strength and post-peak bearing capacity through microcrack propagation and pore expansion. Therefore, the gradual decrease in the residual strength ratio observed in this study further reflects the continuous degradation of structural integrity under freeze-thaw cycles.

Furthermore, the results demonstrate that the stabi-

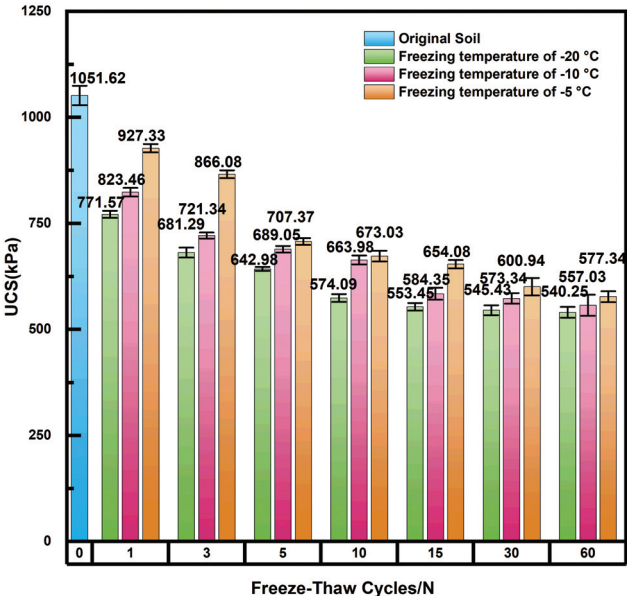

Fig. 3 Unconfined compressive strength (UCS) under different freeze-thaw cycles and freezing temperatures. Error bars represent the standard deviation (SD) of three independent replicates

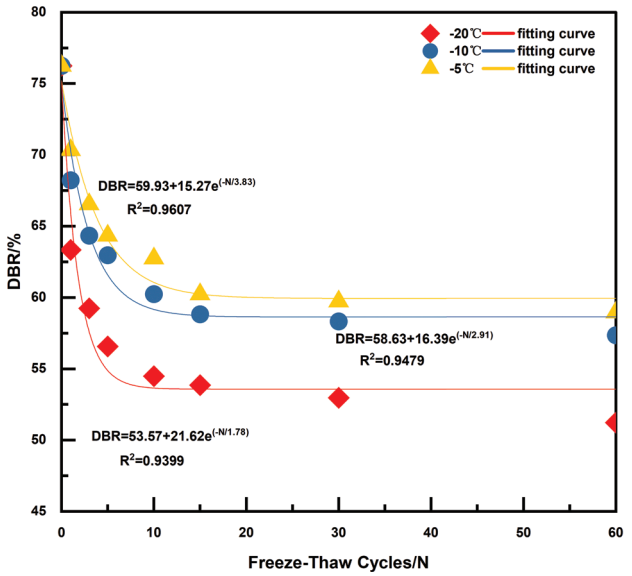

Fig. 4 Changes in residual strength ratio under different freeze-thaw cycles and freezing temperatures

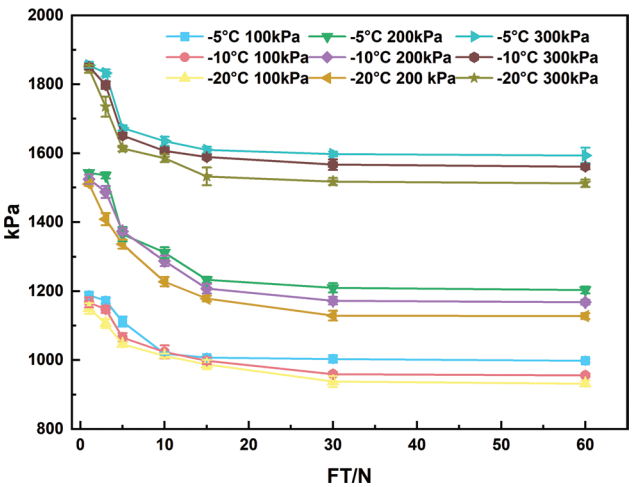

Fig. 5 Variation of shear strength with freeze-thaw cycles under different confining pressures (100, 200, and 300 kPa) at different freezing temperatures. Error bars represent the standard deviation (SD) of three independent replicates

lization treatment can effectively improve the freeze-thaw durability of peat soil. Despite the reduction in unconfined compressive strength (UCS) and residual strength ratio under repeated freeze-thaw cycles, the stabilized peat soil retained considerable strength and exhibited a clear stabilization trend in the later cycles. These findings indicate that the stabilization treatment can mitigate freeze-thaw-induced structural degradation of peat soil and provide a useful reference for its engineering application in foundations and subgrades in seasonally frozen regions.

Figure 5 presents the shear strength evolution of improved peat soil under various freezing temperatures as a function of freeze-thaw cycles at confining pressures of 100, 200, and 300 kPa, respectively. Error bars denote the standard deviation (SD) of triplicate tests. The standard deviation is modest for most groups, and no conspicuous fluctuations in error bars occur during the whole test period, suggesting satisfactory repeatability. Furthermore, the mean values exhibit highly significant intergroup differences, confirming that the experimental results are sufficiently reliable for academic research.

Stress-strain behaviour

Figure 6 presents the stress-strain curves of modified peat soil under freeze-thaw cycles. From the figure, it can be observed that, under different confining pressures, freezing temperatures, and freeze-thaw cycle counts, the trends of the stress-strain curves are similar. Specifically, under varying freeze-thaw cycles, the effects of different freezing temperatures and confining pressures on the shear strength of the modi-

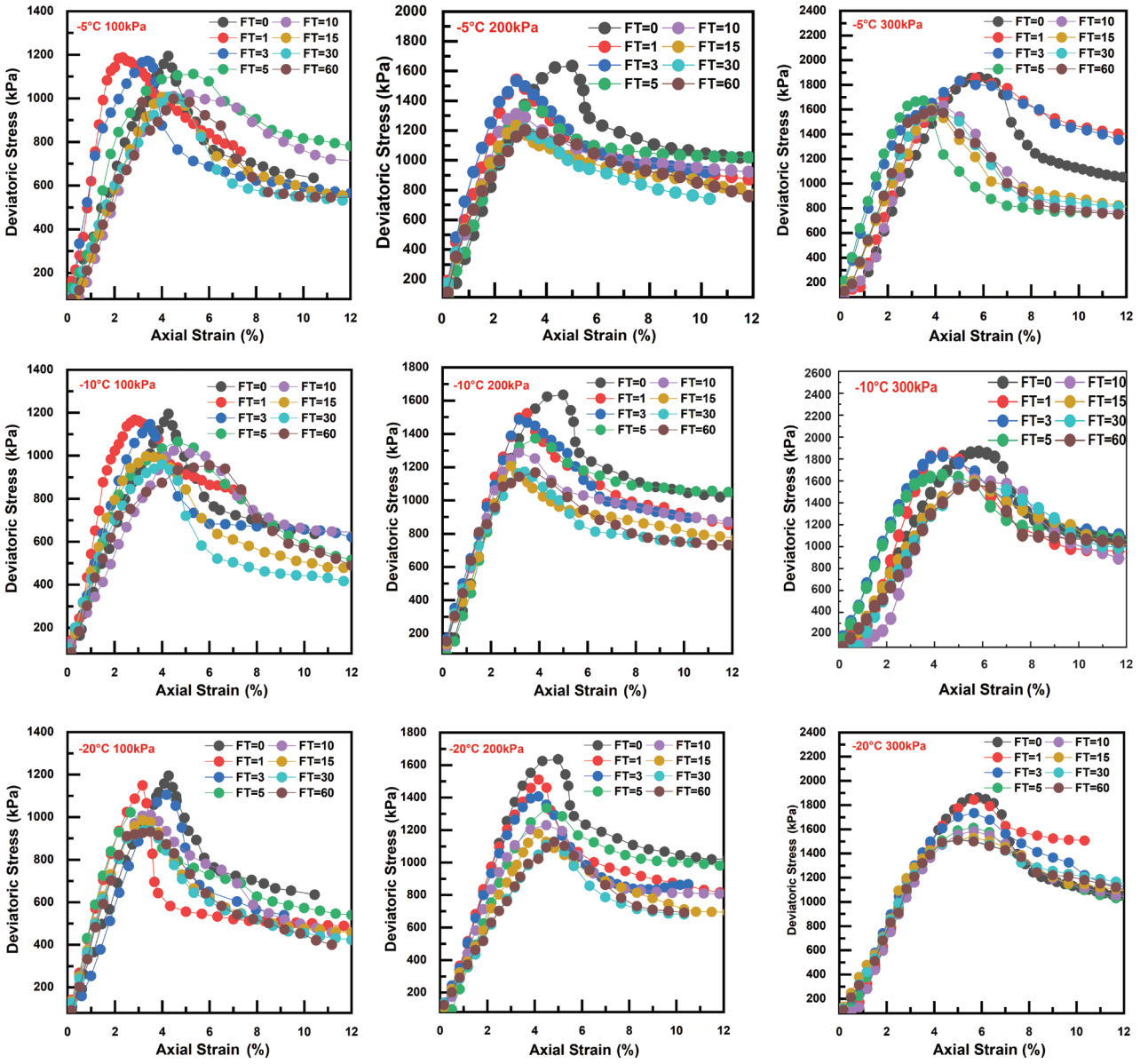

Fig. 6 Stress-strain curves of samples under freeze-thaw conditions at different freezing temperatures and confining pressures

fied peat soil samples are consistent, and the curves all exhibit strain-softening behaviour. After failure, the samples still retain some residual strength, and the failure mode is brittle failure, with shear failure surfaces forming, leading to a rapid drop in strength. The effect of confining pressure on the shape of the stress-strain curve is the most significant. As the confining pressure increases, the peak strength also increases, and the curve gradually transitions from strain-softening to strain-hardening behaviour. At low confining pressures, the specimen reaches peak strength, followed by a rapid strength decline, while under high confining pressure, the curve enters the elastoplastic phase, and the slope becomes relatively gentle.

Ultimate strength and shear strength

Effect of freeze-thaw cycles on the shear strength of stabilized peat soil

To evaluate the impact of freeze-thaw cycles on the mechanical properties of solidified soil, the peak strength values from the stress-strain curves are selected, and the trends in peak strength variation are analyzed to discuss changes in the mechanical properties of the modified soil (Fig. 6). When the freezing temperature was -20°C, the average reduction in peak strength after 1, 3, 5, 10, 15, 30, and 60 freeze-thaw cycles at different confining pressures was 11.74%, 6.73%, 5.85%, 3.61%, 3.56%, 3.39%, and 0.11%, respectively. The experimental results indicate that during the initial freeze-thaw cycles, the deviation in the failure stress of the modified peat soil is significant. However, as the number of cycles increases, the strength decrease becomes less pronounced. This phenomenon occurs because during the freeze-thaw cycles, the water within the sample undergoes a water-ice phase transition, leading to the formation of permeation channels and microcracks within the sample. The cementation and interlocking forces between soil particles weaken (Fang *et al*. 2013). As the number of cycles increases, the internal structure of the sample gradually stabilizes, and the corresponding peak strength also stabilizes (Chen 2024). Similarly, after one freeze-thaw cycle at different freezing temperatures of -5°C and -10°C, the average peak strengths decreased by 1.82% and 1.22%, respectively, compared to the -20°C samples. This suggests that both an increase in freeze-thaw cycles and a decrease in freezing temperature reduce the shear strength of the stabilized soil. This reduction is primarily due to the transformation of water into ice within the sample, which leads to an increase in volume, and while some pore water does not freeze during the freeze-thaw process, this water also gradually decreases as the freezing temperature drops. Consequently, the soil experiences more rapid expansion than contraction, and during melting, the soil structure cannot return to its initial condition. This trend is generally consistent with previous studies on the freeze-thaw deterioration of organic soils, in which the most significant strength loss typically occurs during the initial cycles, followed by a gradual stabilization of mechanical properties. Nevertheless, compared with untreated peat or weakly bonded soils reported in the literature (He *et al*. 2023; Wei *et al*. 2025), the stabilized peat soil in this study still maintained a relatively high peak strength after repeated freeze-thaw actions, indicating that the combined application of stabilizer and fibre reinforcement can effectively mitigate structural damage and retard the accumulation of damage induced by freeze-thaw cycles.

Effect of confining pressure on the shear strength of stabilized peat soil

Figure 7 shows that the differences in peak shear strength of the modified soil under various freezing temperatures are not significant, and the variation trends are consistent. Therefore, the shear strength variation at a freezing temperature of -20°C is further analyzed. Under confining pressures of 100 kPa, 200 kPa, and 300 kPa, after one freeze-thaw cycle, the peak strengths were 1149.89 kPa, 1510.31 kPa, and 1844.83 kPa, respectively. After 60 freeze-thaw cycles, the peak strengths decreased to 931.88 kPa, 1127.85 kPa, and 1512.38 kPa, respectively. The increase in confining pressure enhances lateral confinement, which in turn improves particle compaction, leading to higher overall strength and partially mitigating the damage caused by freeze-thaw cycles. Similar to findings for cement-stabilized or fiber-reinforced frozen soils, increasing confining pressure enhances shear strength mainly by strengthening interparticle contacts and restraining crack propagation (Bao *et al*. 2024; Li *et al*. 2019; Mahya *et al*. 2015; Qiu *et al*. 2024). Nevertheless, strength degradation

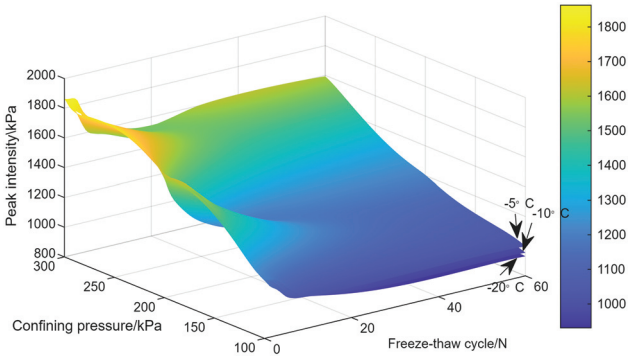

Fig. 7 Variation of failure strength under different freeze-thaw cycles

induced by freeze-thaw cycles was observed under all confining pressures, suggesting that confining pressure can alleviate such damage to a certain extent but cannot fundamentally eliminate the internal structural deterioration caused by repeated freeze-thaw cycles.

Variation of shear strength parameters

As shown in Fig. 8, with increasing freeze-thaw cycles, the cohesion and internal friction angle decrease under different freezing temperatures. For example, at a freezing temperature of -20°C, after the first freeze-thaw cycle, the cohesion exhibits the greatest decrease, with a drop of 10.03%, and after 30 freeze-thaw cycles, the cohesion gradually stabilizes. This result is consistent with the findings from the stress-strain curve analysis. The internal friction angle fluctuated with a maximum variation of 6.72%, but it remained relatively unchanged. These results suggest that the freeze-thaw cycle has the greatest impact on cohesion (Fan *et al*. 2024b). Between 1 and 30 freeze-thaw cycles, as the number of cycles increases, internal structural damage occurs, and the water in the pores generates freezing expansion forces, causing the pore volume to increase and weakening the inter-particle bonding. After 30 freeze-thaw cycles, the internal structure of the soil gradually stabilizes, and cohesion also stabilizes. During the freeze-thaw cycle, the water inside the sample undergoes a cyclic process of liquid-solid-liquid phase transitions, which results in volume expansion and contraction. This expansion-contraction action disturbs the soil skeleton, damaging the particle bonds, reducing the contact area between particles, and macroscopically manifesting as a reduction in cohesion (Peng *et al*. 2024). The test results are consistent with numerous previous freeze-thaw studies (Wang *et al*. 2024; Zheng *et al*. 2025), which indicate that soil cohesion is more sensitive than the internal friction angle under freeze-thaw cycles. This is because cohesion mainly depends on interparticle bonding and structural continuity, which can be readily impaired by ice crystal growth, pore expansion, and elevated pore water pressure. In contrast, the internal friction angle is more closely related to particle shape and frictional contact characteristics, and is therefore less affected unless severe particle rearrangement occurs.

Microstructure of improved peat soil subjected to freeze-thaw cycles

Figure 9 shows the SEM images of cured peat soil under freezing temperatures of -5°C, -10°C, and -20°C after 10 and 30 freeze-thaw cycles. The images reveal significant effects of freeze-thaw cycles on the microstructure of cured peat soil. In samples that have not undergone freeze-thaw cycles (Fig. 9 (g)), the internal structure is compact, with smaller pores between the soil particles, exhibiting a net-like interconnected structure. Macroscopically, the soil appears hardened, dense, and strong. After 10 freeze-thaw cycles, the internal structure begins to loosen. Larger particle aggregates break apart, forming smaller soil particles and debris, and the pores between particles expand. The contact mode between particles shifts to point-to-point and point-to-plane contact (Fig. 9a, b, c). After 60 freeze-thaw cycles, the microstructure shows the development of continuous cracks, creating an open-framework structure. The predominant contact mode becomes point-to-point contact (Fig. 9d, e, f). Moreo-

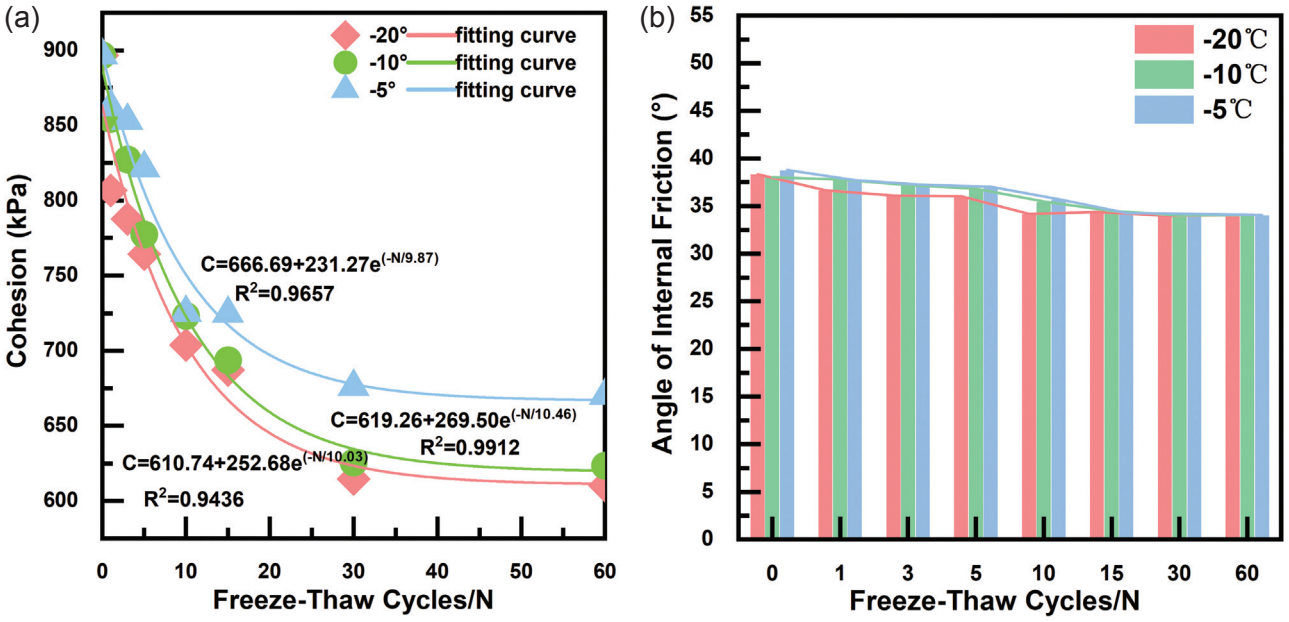

Fig. 8 The variation of shear strength parameters with the number of cycles: (a) The variation law of cohesion under freeze-thaw cycles. (b) The variation law of internal friction angle under freeze-thaw cycles

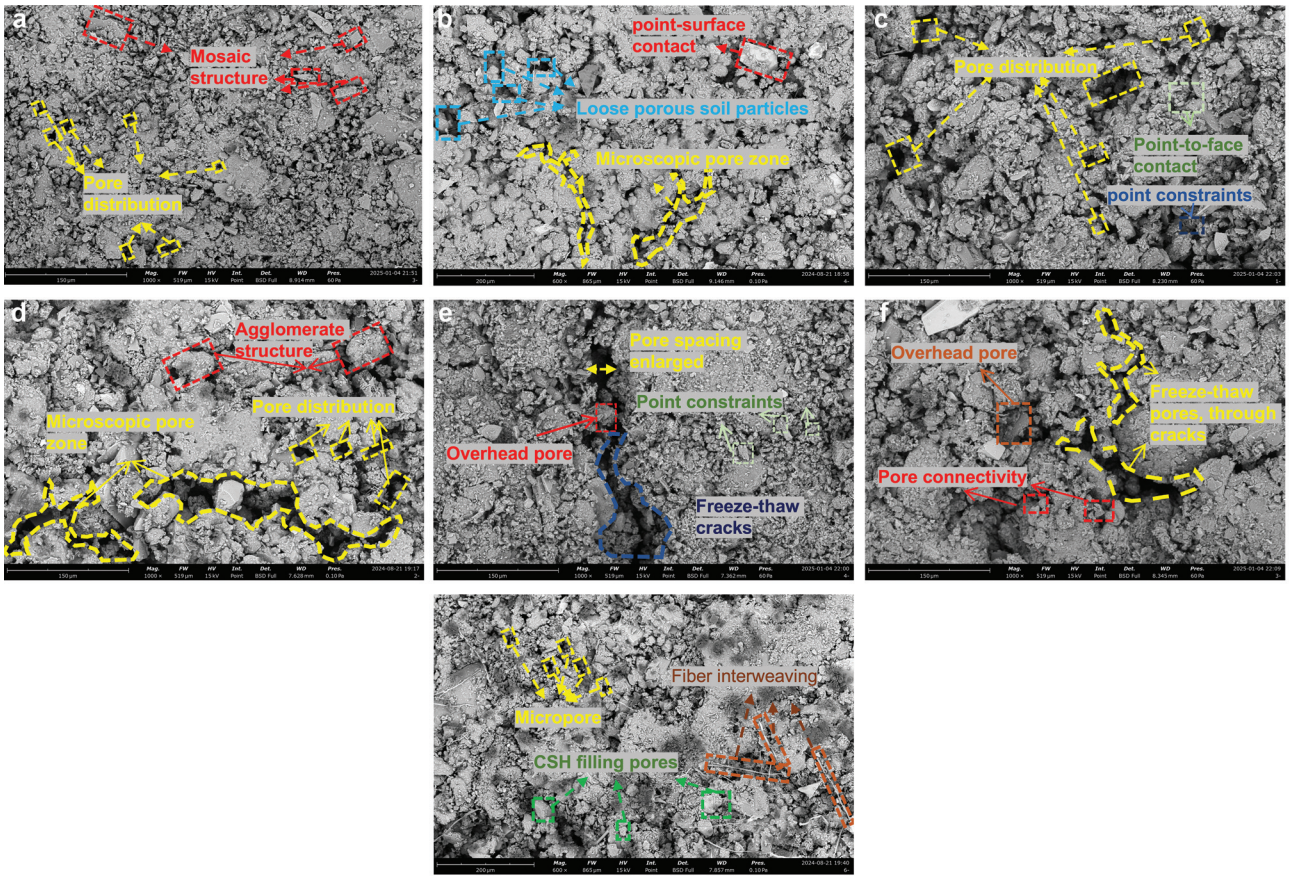

Fig. 9 SEM images of specimens with different freezing temperatures and different numbers of freeze-thaw cycles: (a) Freeze-thaw cycles at-5 °C for 10 times. (b) Freeze-thaw cycles at -10 °C for10 times. (c) Freeze-thaw cycles at -20 °C for 10 times. (d) Freeze-thaw cycles at -5 °C for 60 times. (e) Freeze-thaw cycles at -10 °C for 60 times. (f) Freeze-thaw cycles at -20 °C for 60 times. (g) Freeze-thaw cycle 0 times

ver, as the freezing temperature decreases, the size and number of internal pores in the soil increase, and the cracks inside the sample grow larger in the later stages of freeze-thaw cycles. The previously existing continuous cracks progressively converge, forming larger and more prominent fissures.

This is because, during freeze-thaw cycles, the mechanical properties of the soil change. The cyclic phase transition of the water molecules inside the soil destroys the sample's original stable structure, leading to sliding at the particle connections and weakening the bonding ability. This is macroscopically reflected in the reduced soil strength, although the sample still maintains relatively high mechanical strength (Gao *et al*. 2024).

Peak strength prediction based on PSO-BP neural network

BP neural network

A neural network is a data mapping model that simulates the principles of human brain activity and uses error backpropagation for training. The topology of this model primarily includes an input layer, hidden layer, and output layer (Niu *et al*. 2018). This structure enables the network to systematically learn from a large number of samples and map complex functional relationships with multiple independent or dependent variables. By adjusting the weights and biases of the network, it can approximate complex nonlinear functions without the need for an explicit mathematical expression (Yan *et al*. 2014). As shown in Figure 10, the BP neural network topology adopted in this study was established using the alkali-activated stabilized peat soil dataset. A total of 63 experimental conditions were considered, and three parallel tests were conducted for each condition, resulting in 189 data points in total. Among them, 80% of the dataset (151 samples) was used for model training, while the remaining 20% (38 samples) was used for model testing. The input variables comprised freezing temperature, freeze-thaw cycles, and confining pressure, and the output variable was peak strength. Based on these variables, a three-layer feedforward BP neural network, consisting of an input layer, one hidden layer, and an output layer.

The BP neural network used in this study was con-

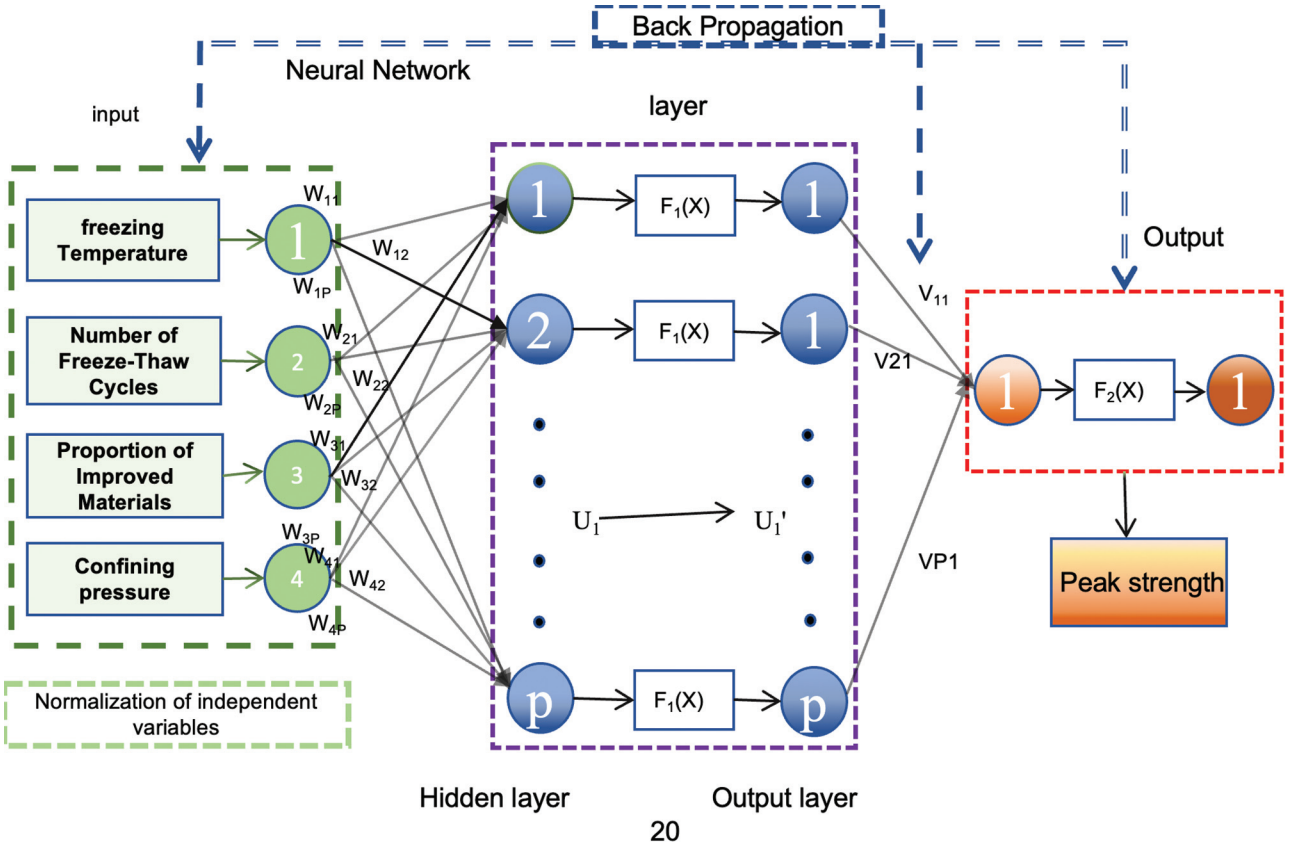

Fig. 10 Schematic diagram of the BP neural network topology

structed as a three-layer feedforward network, consisting of an input layer, a hidden layer, and an output layer. The number of neurons in the hidden layer was set to 20. The hidden layer and the output layer used the tansig and purelin transfer functions, respectively. The network was trained using the Levenberg-Marquardt algorithm (trainlm). The maximum number of training epochs was set to 1000, the learning rate was 0.01, and the training goal was set to 1×10^{-5}. The momentum coefficient was 0.01, the minimum performance gradient was 1×10^{-6}, and the maximum number of validation failures was set to 6.

The number of hidden nodes is determined as 7 by Formula (1), with 20 hidden neurons set. Prior to model training, all samples were randomly shuffled, all samples were randomly shuffled, and 80% of the dataset was used as a training set, while the remaining 20% was used as a testing set to evaluate the predictive performance of the model. Before the data training begins, the independent variables of the sample data are normalized, converting them into the [0,1] range (Shen, Xu 2019).

$$S = \sqrt{m + n} + \gamma \tag{1}$$

$$X_i^* = \frac{X_i - X_{min}}{X_{max} - X_{min}} \tag{2}$$

In the formula, m represents the input neurons, n represents the output neurons, X_i^* and X_i are the normalized and original data, respectively, and X_{max} and X_{min} denote the maximum and minimum values of the sample data.

After normalization, the BP neural network input and output data are set, and the hidden layer variables are processed using the Sigmoid function as the activation function for the hidden layer neurons. The Sigmoid function formula is as follows:

$$f(I) = \frac{1}{1 + e^{-1}} \tag{3}$$

$$I = \sum_{i=1}^{n} \omega_i X_i - T \tag{4}$$

Information is first transferred from the input layer to the hidden layer, with the hidden layer function F1 being:

$$F_1 = f(\sum_{i=1}^{I} \omega_{ij} X_i) \tag{5}$$

The information is then passed from the hidden layer to the output layer, with the output layer function F2 being:

$$\omega_{ij} = \omega_{ij} + \eta F_1 g(\sum_{i=1}^{I} \omega_{ij} F_1) \tag{6}$$

The BP neural network adjusts and updates the weights in the direction of the negative gradient. The error is adjusted in reverse until the algorithm converges, producing the output result. The weights ω_{ij} and υ_{ij} are calculated as:

$$\omega_{ij} = \omega_{ij} + \eta F_1(1 - F_1) X_i g \sum_{i=1}^{l} \omega_{ij} e_k \quad (7)$$

$$v_{ij} = (v_{i1}, v_{i2}, v_{i3} \ldots, v_{im}) \quad (8)$$

In the formula, $k \in N^+$, I represents the number of input nodes, F_1 (x) is the activation function for the hidden layer, F_2 (x) is the activation function for the output layer, and l is the number of hidden layer nodes.

PSO-BP neural network

Although the traditional BP neural network has strong expressiveness and computational capabilities and can replicate the given input-output relationships through repeated learning, this algorithm may lead to overfitting. That is, it performs well on the training data but exhibits poor generalization ability when faced with the test set. The BP neural network's solution process always descends in the direction of the negative gradient, which may result in a local minimum instead of a global minimum. This could prevent finding the optimal solution, and when the network scale is large or the training data is abundant, the training time becomes prolonged, increasing the computational cost.

Therefore, in this study, particle swarm optimization (PSO) was introduced to optimize the key hyperparameters of the BP neural network before final model construction. Specifically, PSO was used to optimize the number of hidden neurons and the learning rate, and the optimized parameter combination was then adopted to establish the final PSO-BP model.

Particle swarm optimization (PSO) is an intelligent evolutionary algorithm inspired by the social behavior of bird flocks or fish schools, where particles communicate information with each other. Each particle seeks its local optimal solution, and ultimately, by merging the local optimal solutions of all particles, the global optimal solution can be found (Wang *et al*. 2024). Compared with the traditional BP neural network, PSO neural network has a faster convergence speed. PSO has a faster convergence speed, and many studies have shown that this algorithm has good applicability in practical engineering (Bao *et al*. 2014; Shariati *et al*. 2019).

Assuming that in an M-dimensional space, a particle swarm consists of N particles searching for the optimal solution within the area, each particle has an initial position X_i and velocity V_i, represented as:

$$V_i = (v_{i1}, v_{i2}, v_{i3} \ldots, v_{im}) \quad (9)$$

$$X_i = (x_{i1}, x_{i2}, x_{i3} \ldots, x_{im}) \quad (10)$$

The position and velocity of each particle are substituted into the objective function, and through continuous iteration, the particle's new position X_{ik} and velocity Vik are updated to determine its fitness value. The fitness value determines the quality of the particle and identifies the best position P_{best} within the search space (Ma *et al*. 2018; Shao *et al*. 2024).

$$V_i^{k+1} = \omega \times v_i^k + c_1 \times r_1 \times [x_{best}^k i - x_i^k] + + c_2 \times r_2 \times [x_{best}^k i - x_i^k] \quad (11)$$

$$X_i^{k+1} = X_i^k + v_i^{k+1} \quad (12)$$

$$P_{best,j} = (p_{i,1}, p_{i,2}, p_{i,3} \cdots, p_{i,n}) \quad (13)$$

$$Q_{best,j} = (q_{i,1}, q_{i,2}, q_{i,3} \cdots, q_{i,n}) \quad (14)$$

In the formula, $X_i^k \in [-x_{\max}, x_{\max}]$; $V_i^k \in [-v_{\max}, v_{\max}]$; $k \in N^+$; $V_i^{k+1}$and X_i^{k+1} represent the position and velocity of the i-th particle in the $(k + 1)$-th iteration; $P_{best,j}$ is the best position for each particle; $Q_{best,j}$ represents the best position of the particle swarm; c_1, c_2 are the learning factors for each particle and the particle swarm, respectively; and r_1, r_2 are random parameters uniformly distributed in the interval [0,1]. In the PSO-BP model, the swarm size was set to 25, and the maximum number of PSO iterations was 30. The inertia weight (w) was set to 0.7, while both cognitive and social learning factors (c_1 and c_2) were set to 1.5. The search range for the number of hidden neurons was defined as 1–50, and the learning rate was set within the range of 0.001–0.1.

Compared to the BP network's gradient descent algorithm, the PSO algorithm is more likely to avoid getting trapped in a local minimum rather than a global minimum, thus achieving the global optimal solution. The flowchart of the PSO-BP neural network algorithm is shown in Fig. 11.

Comparison of failure strength simulation

This study introduces k-fold cross-validation (k = 10) into the neural network model to evaluate

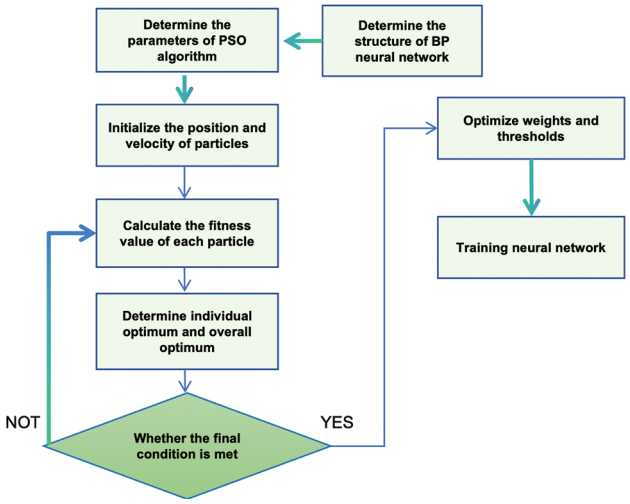

Fig. 11 Process of PSO-BP neural network

and compare its accuracy, stability, and generalization ability. Specifically, the entire dataset was randomly divided into ten approximately equal subsets. In each iteration, one subset was used as a testing set, while the remaining subsets were used as a training set. This process was repeated ten times. The final generalization performance of the model was represented by the average of the results from the ten validations. This approach helps to minimize the influence of random data partitioning and provides a more objective evaluation of the model's reliability.

On this basis, a multiple linear regression (MLR) model was introduced to compare the predictive performance of the neural network. For the MLR model, 80% of the samples were used for training, while the remaining 20% were used for testing.

The model performance was evaluated using four statistical indicators, namely MAE, MAPE, RMSE, and R^2. Among them, MAE, MAPE, and RMSE were used to quantify prediction errors, whereas R^2 was used to assess the goodness of fit between predicted and measured values (Qu *et al*. 2023). The corresponding equations are given as follows:

$$Y = \beta_0 + \beta_1 Z_1 + \beta_2 Z_2 + \cdots + \beta_f Z_f + \varepsilon \tag{15}$$

$$Y = X\beta + \varepsilon \tag{16}$$

$$\hat{\beta} = (X^T X)^{-1} X^T Y \tag{17}$$

where Y is the predicted strength, β_0 is the intercept, $\beta_i (i = 1, 2, \ldots, f)$ are the regression coefficients, Z_i are the standardized input variables, $\hat{\beta}$ represents the estimated vector of regression coefficients, and ε is the random error term.

$$MAE = \frac{1}{m}\sum_{i=1}^{m} |Y_i - Y_i^*| \tag{18}$$

$$MAPE = \frac{1}{m}\sum_{i=1}^{m} \left|\frac{Y_i - Y_i^*}{Y_i}\right| \tag{19}$$

$$RMSE = \sqrt{\frac{1}{m}\sum_{i=1}^{m}(Y_i - Y_i^*)^2} \tag{20}$$

$$R^2 = 1 - \frac{\sum_{i=1}^{n}(Y_i^* - \bar{Y})}{\sum_{i=1}^{n}(Y_i - \bar{Y})} \tag{21}$$

In the formula, Y_i^* is the predicted failure strength, $\bar{Y}$ is the average of the actual failure strength, and Y_i represents the actual failure strength for the i-th sample.

The smaller the values for MAE, MAPE, and RMSE and the closer R^2 is to 1, the stronger the relationship between the actual compressive strength and the model's predicted value. Smaller error values and higher R^2 indicate a more precise fitting of the model, and vice versa for lower correlations (Ma *et al*. 2023).

As shown in Fig. 12, among the three models, the PSO-BP network exhibited the best predictive performance, followed by the BP model, while the MLR model performed the worst. The relatively low R^2 values of the MLR model (R^2 = 0.8984 for the training set, and R^2 = 0.8878 for the testing set) can be attributed to its limitation to simple linear relationships. In contrast, the mechanical behaviour of alkali-activated stabilized soil under freeze-thaw cycles involves a staged evolution associated with ice-water phase transitions, which cannot be captured by a linear model.

Compared with the MLR model, the BP neural network substantially improved the prediction accuracy, with R^2 values exceeding 0.9 for both the training and testing sets. However, the predictive performance on the testing set was noticeably lower than that on the training set. Under small-sample training conditions, although the BP network is capable of handling complex nonlinear relationships, it is prone to being trapped in local optima, exhibits a limited generalization capability, and is sensitive to the division of the dataset.

Compared with the BP neural network, the PSO-BP model achieved superior predictive performance. For the training set, the R^2, MAE, RMSE, and MAPE values were 0.9760, 32.9617 kPa, 43.2382 kPa, and 2.5633%, respectively. For the testing set, the corresponding values were 0.9625, 41.5050 kPa, 50.0286 kPa, and 3.3911%, respectively. Compared with the traditional BP model, the PSO-BP model reduced MAE, RMSE, and MAPE by 15.9%, 23.1%,

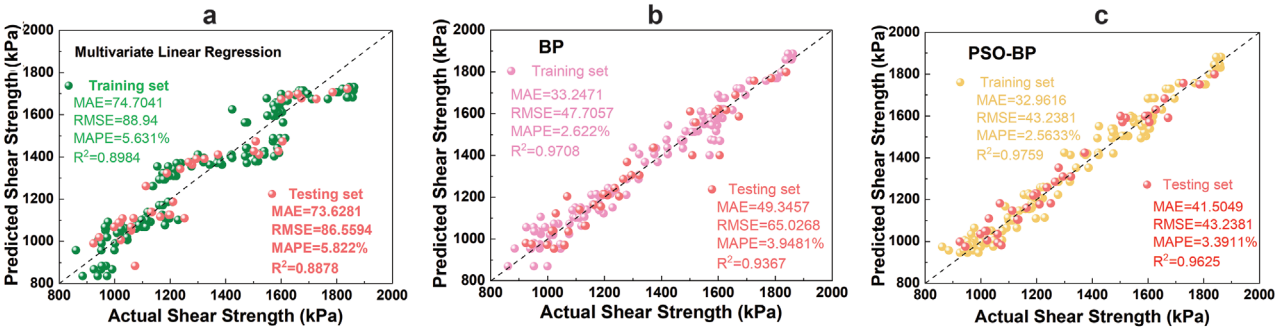

Fig. 12 Comparison of prediction results from different models: (a) MLR prediction results. (b) BP network prediction results. (c) PSO-BP network prediction results

and 14.1%, respectively, while increasing the R^2 value from 0.9367 to 0.9625.

The particle swarm optimization (PSO) algorithm enables the search for more suitable parameter combinations within a defined range by incorporating both individual best and global best solutions. The difference between the R^2 values of the training and testing sets is only 0.0135, indicating that the PSO-BP model exhibits a better generalization capability than the conventional BP neural network.

Although the R^2 value of the PSO-BP training set reaches as high as 0.9936, which may raise doubts about the model validity, the R^2value of the test set remains high at 0.9625, close to that of the training set. A small difference between the two R^2 values indicates that the model does not exhibit serious overfitting and has a good generalization ability.

Residual analysis (Fig. 13) was further conducted to clarify the differences in fitting performance and generalization ability among the three models. The residuals of the MLR model exhibit significant fluctuations and high dispersion for both the training and testing sets, indicating that a simple linear model is insufficient to accurately predict the actual failure strength. Compared with the MLR model, the BP neural network shows some degree of convergence in the residuals; however, the residuals in the testing set still display considerable scatter and large fluctuations.

In contrast, the PSO-BP model demonstrates relatively small residual variations in both the training and testing phases, with residuals distributed symmetrically around zero. Considering the MAE, RMSE, R^2, and residual analysis together, the particle swarm optimized neural network not only improves the fitting accuracy but also confines the prediction errors within a relatively narrow range. Therefore, it exhibits superior accuracy and generalization capability for predicting the strength of stabilized soil under complex conditions with limited sample data.

The dataset used in this study is relatively small, which may raise concerns regarding the applicability of the model to future scenarios. To address this issue, a simpler model, namely multiple linear regression (MLR), was employed as a baseline for comparison. In addition, a 10-fold cross-validation strategy was adopted to enhance the reliability and stability of the models.

Although neural network models generally require larger datasets, the results of this study demonstrate that they can effectively capture the complex nonlinear relationships among variables, which are difficult to describe using traditional linear approaches. Therefore, the application of the PSO-BP model to simulate the shear strength of stabilized peat soil under freeze-thaw conditions is considered reasonable.

Nevertheless, a limited sample size may still affect the generalization capability of the model. To mitigate this limitation, future studies should expand the experimental dataset to further improve the predictive accuracy of the model.

CONCLUSIONS

Through freeze-thaw cycle tests, unconfined compressive strength tests, consolidated-undrained shear tests, scanning electron microscope (SEM) tests, and PSO-BP neural network strength predictions of cured peat soil, the following conclusions were drawn:

1. Both the unconfined compressive strength and the shear strength of stabilized peat soil exhibit varying degrees of degradation under freeze–thaw cycles. With an increasing number of freeze-thaw cycles, the strength further deteriorates, with the most significant reduction occurring in the early stages, followed by a relatively stable and higher strength in the later stages. This indicates that alkali activation has a positive effect on enhancing the freeze-thaw resistance of the soil.

2. The scanning electron microscopy (SEM) results provide a microscopic perspective on the freeze-thaw damage mechanism. With increasing freeze-thaw cycles, the stabilized peat soil undergoes repeated ice-water phase transitions, leading to a progressively

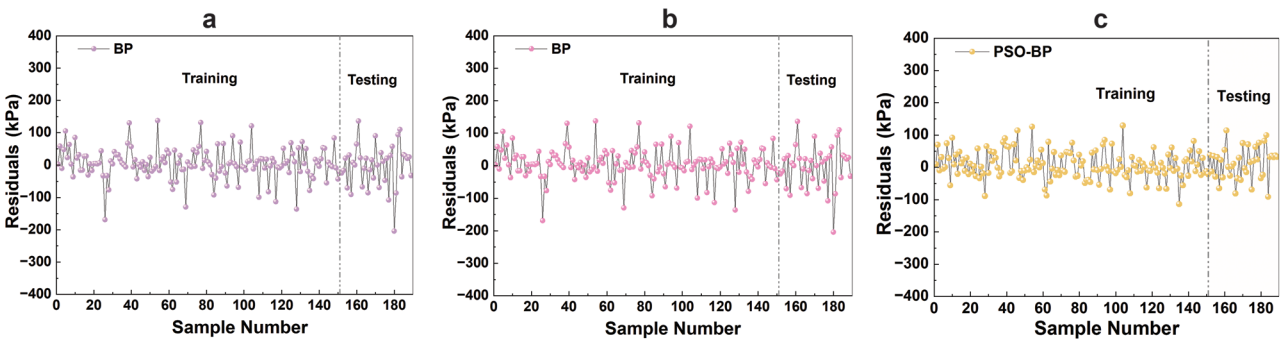

Fig. 13 Comparison of residual results of different models: (a) MLR residual results. (b) BP network residual results. (c) PSO-BP network residual results

looser internal structure, the expansion of cracks and pores, and the weakened interparticle bonding. These microstructural changes are reflected macroscopically as a reduction in strength.

3. In this study, a multiple linear regression (MLR) model, a BP neural network model, and a PSO-BP neural network model were employed, with the neural network models incorporating the 10-fold cross-validation. Comparative results show that the PSO-BP neural network achieves superior prediction accuracy and generalization capability compared with the other two models. This indicates its strong application potential and provides a useful reference for predicting the shear strength of peat soil in seasonal frozen regions.

ACKNOWLEDGMENTS

This study was supported by the National Natural Science Foundation of China (U23A20651). The authors would like to express their sincere gratitude to the two anonymous reviewers for their insightful comments and constructive suggestions, which have significantly improved the quality of this manuscript.

Conflict of interests. The authors declare that they have no known competing financial interests or personal relationships that could have appeared to influence the work reported in this paper. No artificial intelligence (AI) technologies were used in the preparation of this manuscript.

REFERENCES

Bao, W.X., Qin, C., Li, W., Liu, Y.L., Chen, R. 2024. Study on the Mechanical Characteristics of Salinized Silt Soil with Low Liquid Limit under Freeze-Thaw Cycle. *Chinese Journal of Underground Space and Engineering 20(04)*, 1223–1235. https://doi.org/10.20174/j.JUSE.2024.04.16 [In Chinese].

Bao, Y.K., Xiong, T., Hu, Z.Y. 2014. PSO-MISMO Modeling Strategy for MultiStep-Ahead Time Series Prediction. *IEEE Transactions on Cybernetics 44(5)*, 655–668. https://doi.org/10.1109/tcyb.2013.2265084

Chai, S.Y., Zhang, L.K. 2023. Study on Damage Mechanism of Alkali Activated Fly Ash Mineral Powder Modified Expansive Soil Under Drying Wetting Freezing Thawing Cycles. *Engineering Mechanics* 1–12 [In Chinese].

Chen, X.Y. 2024. Experimental Study on Strength and Permeability of CMC Improved Loess under Freeze-Thaw Cycles. *China Rural Water and Hydropower* 1–13 [In Chinese].

Chen, Z.F., Chen, H.E., Li, J.F., Li, H., Ma, W.L. 2019. Study on the Changing Rules of Silty Clay's Pore Structure under Freeze-Thaw Cycles. *Advances in Civil Engineering 2019*, 7493872. https://doi.org/10.1155/2019/7493872

Ding, S.J., Li, S.M., Kong, S., Li, Q.Y., Yang, T.H., Nie, Z.B., Zhao, G.W. 2024a. Changing of mechanical property and bearing capacity of strongly chlorine saline soil under freeze-thaw cycles. *Scientific Reports 14(1)*, 6203. https://doi.org/10.1038/s41598-024-56822-8

Ding, X.S., Zhang, L.K., Fan, P.P. 2024b. Strength degradation law and nonlinear model of remolded loess under dry-wet freeze-thaw cycles condition. *Rock and Soil Mechanics 45(S1)*, 324–336. https://doi.org/10.16285/j.rsm.2023.1904 [In Chinese].

Fan, L.F., Zhong, W.L., Wang, G., Xi,Y. 2023. Optimal slag content for geopolymer composites under freeze-thaw cycles with different freezing temperatures. *Journal of Zhejiang University: Science A 24(4)*, 366–376. https://doi.org/10.1631/jzus.A2200437

Fan, J.K., Yue, Z.R., Han, Z.H., Sun, T.C., Hu, T.F., Zhang, S. 2024a. Study on prediction model of strength deterioration of moraine soil under high frequency freeze-thaw cycles. *Journal of Glaciology and Geocryology 46(02)*, 602–611 [In Chinese].

Fan, P.P., Zhang, L.K., Ding, X.S. 2024b. Deterioration law of shear and compression characteristics of collapsible loess under dry-wet and freeze-thaw cycles. *Rock and Soil Mechanics 45(07)*, 2050–2060. https://doi.org/10.16285/j.rsm.2023.1281 [In Chinese].

Fang, X.W., Shen, C.N., Li, C.H., Wang, L., Chen, Z.H. 2013. Quantitative Analysis of Microstructure Characteristics of Pucheng Loess in Shaanxi Province. *Chinese Journal of Rock Mechanics and Engineering 32(09)*, 1917–1925 [In Chinese].

Feng, D.C., Yi, J.Y., Wang, D.S., Chen, L.L. 2010. Impact of salt and freeze-thaw cycles on performance of asphalt mixtures in coastal frozen region of China. *Cold Regions Science and Technology 62(1)*, 34–41. https://doi.org/10.1016/j.coldregions.2010.02.002

Gao, Y., Ma, Y.X., Yang, F.H., Li, H. 2024. Collapsible Deformation and Microscopic Mechanism of Loess in Seasonally Frozen Soil Region. *Science Technology and Engineering 24(34)*, 14778–14786 [In Chinese].

He, Y.Y., Xu, Y., Lv, Y., Nie, L., Kong, F.S., Yang, S.T., Wang, H., Li, T.T. 2023. Characterization of unfrozen water in highly organic turfy soil during freeze-thaw by nuclear magnetic resonance. *Engineering Geology 312*. https://doi.org/10.1016/j.enggeo.2022.106937

Hou, B., Dang, F.N., Peng, C.H., Liu, Y., Zhu, W.W., Yao, Y., Li, J.Y. 2025. Study on freeze-thaw resistance of cellulose modified loess based on complex stress state. *Construction and Building Materials 458*, 139659. https://doi.org/10.1016/j.conbuildmat.2024.139659

Kalkan, E., Yarbasi, N., Bilici, O., Karimdoust, S. 2022. Effects of quartzite on the freeze-thaw resistance of clayey soil material from Erzurum, NE Turkey. *Bulletin of Engineering Geology and the Environment 81(5)*, 191. https://doi.org/10.1007/s10064-022-02691-2

Kan, L.L., Dai, W., Dai, L.Q. 2024. Frost resistance properties of fiber reinforced alkali-activated slag/fly ash composites. *Materials Reports 39(15)*, 1–14 [In Chinese].

Li, J., Wang, F.C., Yi, F., Wu, F.Y., Liu, J.S., Lin, Z.H. 2019. Effect of Freeze-Thaw Cycles on Triaxial Strength Property Damage to Cement Improved Aeolian Sand (CIAS). *Materials (Basel, Switzerland) 12*. https://doi.org/10.1007/s13296-015-6017-2

Li, Z.B., Su, S.A., Zhang, X.D., Liu, L.J., Liu, C.L., Ding, L., Xu, F.L., Li, Z.W. 2023. Experimental Study on Roadbed Filling Improvement of Saline Soil in Northeast China under Freeze-Thaw Cycle. *Forest Engineering 39(02)*, 139–147 [In Chinese].

Ma, T., Ma, Y., Huang, X.M. 2023. Optimal combination of key parameters of intelligent compaction based on multiple nonlinear regression. *Journal of Jilin University (Engineering and Technology Edition) 53(07)*, 2067–2077. https://doi.org/10.13229/j.cnki.jdxbgxb.20211010 [In Chinese].

Ma, Y.B., Du, X.Y. 2018. Effects of CaO Addition on the Iron Recycling from Nickel Slags by Oxidation-Magnetic Separation. *Metals 8(11)*, 956. https://doi.org/10.3390/met8110956

Mahya, R., Abolfazl, E., Mahmoud, G. 2015. Effects of freeze-thaw cycles on a fiber reinforced fine grained soil in relation to geotechnical parameters. *Cold Regions Science and Technology 120,* 127–137. https://doi.org/10.1016/j.coldregions.2015.09.011

Niu, J.C., Han, L.T., Li, S.J., Han, J.B., Liu, J.Z. 2018. Research on Shield Cutting Tool Configuration Based on PSO-BP Neural Network. *Journal of Mechanical Engineering 54(10)*, 167–172 [In Chinese].

Peng, Y.T., He, W.Y., Li, L.,Wang, Z.L. 2024. Experimental Study on Shear Characteristics of Silt under Different Temperature-humidity Freeze-thaw Cycles. *Geotechnical Engineering Technique 38(02)*, 203–210 [In Chinese].

Qiu, E.X., Pan, H.Y., He, Q.L., Sun, X.W., Wan, X.S., Zhang, R., Wang, Z.S. 2024. Tests on the Mechanical Properties of Moraine Soils under Freeze-Thaw Conditions and the Modified Duncan-Zhang Model. *Journal of Engineering Geology 32(03)*, 772–784. https://doi.org/10.13544/j.cnki.jeg.2023-0351 [In Chinese].

Qu, G.L., Yan, Z.W., Zheng, M.L., Liu, H., Yuan, Y.M. 2023. Performance prediction of porous concrete based on neural network and regression analysis. *Journal of Jilin University (Engineering and Technology Edition)*, 1–13. https://doi.org/10.13229/j.cnki.jdxbgxb.20230239 [In Chinese].

Shao, L., Li, P.Q., Wang, B.J. 2022. Influence of Freeze-thaw Cycle on Strength of Soft soil Solidified by Alkali-activated Ground Granulated Blast Furnace Slag. *Journal of Highway and Transportation Research and Development 39(01)*, 40–47 [In Chinese].

Shao, M., Pan, Z.Z., Sun, J.W., Shao, X.Z., Yi, C.X. 2024. Short-Term Tidal Current Speed Prediction Based on EMD-PSO-BP Model. *Periodical of Ocean University of China 54(11)*, 134–141. https://doi.org/10.16441/j.cnki.hdxb.20220321 [In Chinese].

Shariati, M., Mafipour, M.S., Mehrabi, P., Bahadori, A., Zandi, Y., Salih, M.N.A., Nguyen, H., Dou, J., Song, X., Poi-Ngian, S. 2019. Application of a Hybrid Artificial Neural Network-Particle Swarm Optimization (ANN-PSO) Model in Behavior Prediction of Channel Shear Connectors Embedded in Normal and High-Strength Concrete. *Applied Sciences-Basel 9(24)*, 5534. https://doi.org/10.3390/app9245534

Shen, J.R., Xu, Q.J. 2019. Prediction of interlayer shear strength parameters for RCC dams using artificial neural network and fuzzy logic system. *Journal of Tsinghua University (Science and Technology) 59(05)*, 345–353. https://doi.org/10.16511/j.cnki.qhdxxb.2018.25.058 [In Chinese].

Shi, X., Yang, P., Li, L., Geng, X.Y., Liu, X., Zhao, K.L. 2024. Strength and microscopic pore structure characterization of cement-fly ash stabilized organic soil under freeze-thaw cycles. *Construction and Building Materials 420.* https://doi.org/10.1016/j.conbuildmat.2024.135635

Sun, Y.D., Li, C., Bi, Q.Y., Li, J.W., Huang, J.K., Shi, M.Y., Cui, H.Z. 2025. A machine learning-assisted method for evaluating the strength of silty clay solidified with industrial waste under freeze-thaw cycles. *Construction and Building Materials 493*, 143070–143070. 10.1016/j.Conbuildmat.2025.143070.

Tang, S.Y., Xia, M., Cui, Y.Y., Chang, Z.K., Ren, G.M. 2027. Strength and Microstructure of Alkali-Activated Solid Waste–Based Peat Soil System. Manuscript in preparation.

Wan, S.W., Xu, P., Xu, J., Xing, G.W., Chen, S.B. 2018. Experimental Study on Residual Strength of Concrete after High Temperature. *Science Technology and Engineering 18(06)*, 316–320 [In Chinese].

Wang, J.W., Wang, J., Liu, S., Pan, Z.Y. 2022. Construction Period Prediction of Open-cut Subway Station Based on PSO-BP. *Journal of Civil Engineering and Management 39(02)*, 7–11+18 https://doi.org/10.13579/j.cnki.2095-0985.2022.20210357 [In Chinese].

Wang, R.H., Jing, Z.H., Luo, H., Bao, S., Jia, J.R., Zhan, X.Y. 2024. Effect of freeze–thaw cycles on root–Soil composite mechanical properties and slope stability. *PLOS ONE 19*. https://doi.org/10.1371/journal.pone.0302409

Wei, H., Yao, Z.M., Wang, X., Song, Z.H. 2025. The mechanical properties of frozen peat soil under true triaxial testing and intelligent constitutive modeling based on prior information. *Cold Regions Science and Technology 236.* https://doi.org/10.1016/j.coldregions.2025.104496

Yan, C.L., Hao, Y.X., Liu, K.G. 2014. Fatigue life prediction of materials based on BP neural networks optimized by genetic algorithm. *Journal of Jilin University (Engineering and Technology Edition) 44(06)*, 1710–1715. https://doi.org/10.13229/j.cnki.jdxbgxb201406027 [In Chinese].

Yang, A.W., Yang, S.P., Zhong, X.K., Zhang, X.W. 2022. Mechanical Properties and Structural Evolution of Sludge-cured Lightweight Soils Subjected to Freeze-

thaw Cycles. *Ksce Journal of Civil Engineering 26(11)*, 4478–4488 https://doi.org/10.1007/s12205-022-2172-0

Yao, C., Hu, G., Chen, Q., Wu, J. 2024. Prediction on the freeze-thaw resistance of a one-part geopolymer stabilized soil by using deep learning method. *Case Studies in Construction Materials 21*, e03530-e03530 10.1016/j.Cscm.2024.E03530

Zhang, Y.W., Han, C.P. 2024. Mechanical Properties and Microstructure of Dispersed Soils under Different Freeze-thaw Cycles. *Forest Engineering 40(03)*, 204–211 [In Chinese].

Zhao, J.L., Yang, P., Li, L., Zhang, T., Wang, H.B. 2024. Influence of freeze thaw on stress-strain characteristics and microstructure of cement and fly ash stabilized organic soil. *Geomechanics and Engineering 39(6)*, 529–546. https://doi.org/10.12989/gae.2024.39.6.529

Zheng, F., Xue, X.L., Song, Z.P., Zhang, Y.W., Liu, H.K. 2025. The Influence of Freeze-Thaw Cycles on the Mechanical Properties of Loess Under Temperature Variations. *Buildings 15(11)*, 1806. https://doi.org/10.3390/buildings15111806